第 50 卷 第 21 期/2023 年 11 月/中国激光 研究论文

中国激光

PEG 修饰的硅量子点应用于细胞的二次谐波成像

陈蕾[1*]，向进[2]，赵年[3**]，陈同生[4]

[1]佛山科学技术学院物理与光电工程学院，广东 佛山 528000；

[2]重庆大学光电工程学院，光电技术及系统教育部重点实验室，重庆 400044；

[3]湘潭大学物理与光电工程学院，湖南 湘潭 411105；

[4]华南师范大学生物光子学研究院，广东省激光生命科学重点实验室，广东 广州 510631

摘要 二次谐波成像作为一种高空间分辨率和高穿透深度的非线性光学成像技术，可以避免荧光成像中由能量吸收导致的光漂白和饱和吸收等问题，在临床诊断和生物医学领域具有广阔的应用前景。笔者引入了一种具有中心反演对称破缺、高非线性光学效应的材料——硅量子点作为二次谐波探针，同时为了增强硅量子点的生物亲和性并减少其表面氧化，利用聚乙二醇对硅量子点进行修饰，并将其作为生物探针探究了其在人肝癌细胞（HepG2）中的二次谐波成像效果。通过与双光子荧光成像结果进行对比发现，基于聚乙二醇修饰的硅量子点的二次谐波成像技术具有可靠性和稳定性。本研究对未来硅量子点在分子成像、药物递送和干细胞治疗中的应用具有积极的推动作用。

关键词 非线性光学；二次谐波成像；硅量子点；人肝癌细胞；生物探针

中图分类号 O734+.1 **文献标志码** A **DOI**：10.3788/CJL230983

1 引 言

随着飞秒激光器的诞生，基于飞秒激光的非线性光学成像技术成为生命科学研究中的重要手段[1-4]。非线性光学成像包括相干反斯托克斯拉曼（CARS）成像、双光子荧光（TPL）成像和二次谐波（SHG）成像等[5-8]。SHG 是指两个频率相同的光子与非线性介质相互作用产生能量是初始光子两倍的光子的过程[9]。相比于 CARS 成像和 TPL 成像，SHG 成像在生物医学领域具有独特优势[10-11]：1）在非中心对称的晶体材料中，二阶非线性效应一般远大于三阶非线性效应，因此 SHG 光谱更窄、强度更高；2）SHG 可避免 TPL 成像中由能量吸收引起的光漂白和光毒性；3）SHG 利用近红外区光激发样品，因此对组织的穿透深度较大。在生物医学成像研究中，能够产生 SHG 信号的介质主要分为两类：生物组织和外源探针。1971 年，Fine 和 Hansen[12]在胶原组织中首次检测到了 SHG 信号；1978 年，Cannaway 和 Sheppard[13]利用光学扫描显微镜获得了 SHG 影像；1986 年，Freund 等[14]对大鼠尾巴肌腱进行了 SHG 成像。之后，研究人员将 SHG 成像应用于监测肿瘤胶原蛋白和肌肉组织中肌动球蛋白的动态变化[15-21]。虽然无标记的内源性 SHG 成像避免了外源性染料对生物体的潜在毒性，然而大多数内源性物质的 SHG 信号强度较弱，因此，研究人员引入了各种非线性光学材料，并将其制备成纳米成像探针对生物样本进行标记，以便用于生物医学成像研究。目前，多种无机 SHG 纳米探针如钛酸钡、铌酸锂、氧化锌已被证实能诱导较强且稳定的 SHG 信号[22-26]。然而，这些含有金属元素的无机晶体材料通常具有较大的尺寸（直径约 100 nm），它们在生物相容性和靶向标记能力等方面很难满足医学研究和临床应用的要求。此外，有机材料也表现出了优良的 SHG 性质[27-29]，但有机染料在 SHG 产生过程中通常伴随着双光子荧光发射，容易对生物组织造成光损伤。因此，亟须开发一种尺寸更小、生物相容性更高、光稳定性更好的非金属 SHG 探针。

与传统的有机分子和无机分子材料相比，量子点具有非线性效应强、激发光谱宽、发射光谱窄、光化学稳定性高、量子局限效应明显等优点，被认为是生物探针的理想材料[30-33]。Qi 等[34]使用硼掺杂的石墨烯量子点来追踪干细胞，Nayfeh 等[35]使用硅量子点（SiQDs）重组的微晶薄膜来观察 SHG 成像。迄今为止，鲜有在不进行任何结构重构的情况下研究量子点光学应用的研究报道，尤其是 SHG 成像。笔者制备了一种具有高度生物相容性、无毒且制备方式简单的被聚乙二醇（PEG）修饰的 SiQDs，它能够产生强烈的用于生物标记的 SHG 信号。笔者首先介绍了 SiQDs 的制备和特

收稿日期：2023-07-03；**修回日期**：2023-07-22；**录用日期**：2023-08-01；**网络首发日期**：2023-08-15

基金项目：国家自然科学基金（62105062）

通信作者：*chenl@ fosu.edu.cn；**nzhao@xtu.edu.cn

性，并通过时域有限差分（FDTD）法对比了 SiQDs 和单晶硅纳米颗粒（SiNP）的非线性光学效应，揭示了 SiQDs 强的局域光场束缚能力；随后，笔者使用所制备的 SiQDs 标记人肝癌细胞（HepG2），并分别通过 SHG 和 TPL 进行细胞成像，成像结果验证了所制备的 SiQDs 作为生物探针在 SHG 细胞成像应用中的可行性。

2 材料与方法

2.1 SiQDs 的制备与表征

本实验使用的非线性材料——PEG 修饰的 SiQDs 是通过还原硅氧键直接合成然后通过有机配体进行修饰得到的。具体制备过程如下[36]：1）向 40 mL 超纯水中加入 10 mL 3-（氨基丙基）-三甲氧基硅烷（APTMS），持续搅拌，温度保持在 40 ℃；2）向上述混合溶液中加入 12.5 mL 浓度为 0.1 mol/L 的抗坏血酸钠（其中 APTMS 为前驱体，抗坏血酸钠为还原剂），搅拌 3 h，再在 10000 r/min 的转速下离心 10 min，去除较大的沉淀物；3）将生成的溶液在透析袋中透析 3 d（截留分子量为 1000），以进一步净化 SiQDs；4）将获得的 SiQDs 和 NH2-PEG1000 超声处理 6 h，获得水溶性 PEG 修饰的 SiQDs。

从图 1（a）所示的 SiQDs 的透射电子显微镜（TEM）照片可以看出，利用还原硅烷法制备的 SiQDs 近似为球形，且其粒径分布较为均匀，平均直径为（2±0.5）nm，没有发现 SiQDs 聚集现象。图 1（b）为高分辨率 TEM（HR - TEM）图像，其中白色虚线圆圈中是 SiQDs。由图 1（b）可知 SiQDs 具有晶面间距约为 0.189 nm 的晶体结构，其可与硅的（220）晶面很好地对应。对样品进行能量色散 X 射线能谱（EDS）分析，分析结果如图 1（c）所示。可见，SiQDs 由 Si、C 和 O 三种元素组成，Cu 信号是由测量中使用的铜栅格诱导产生的。该结果排除了溶液中其他杂质的存在。

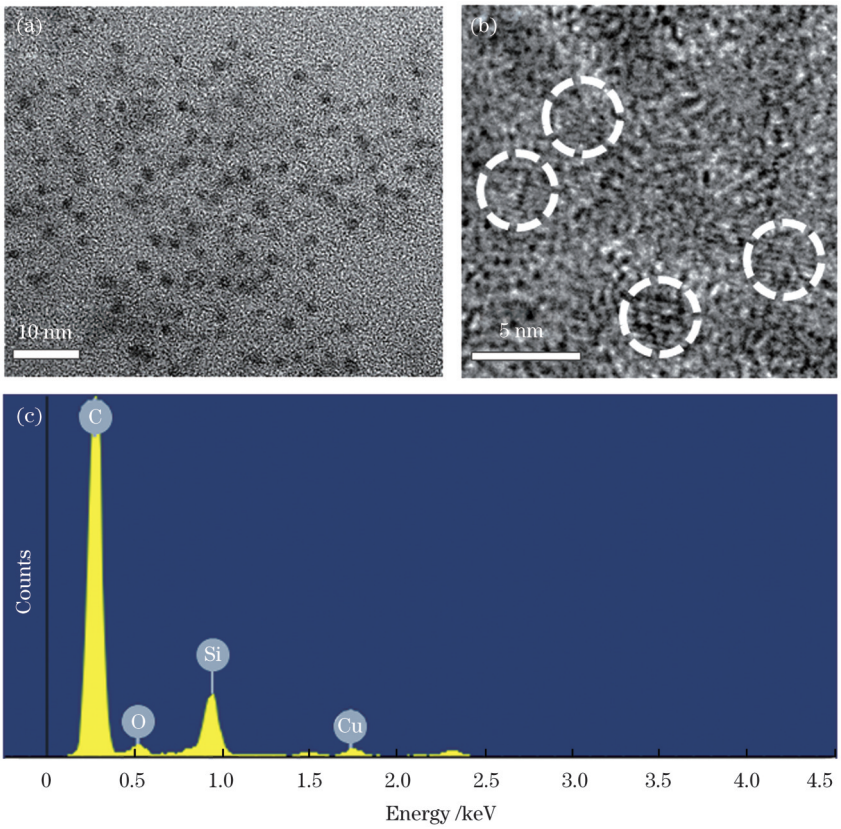

图 1 PEG 修饰的 SiQDs 的结构表征。（a）TEM 图像；（b）HR-TEM 图像；（c）EDS 谱

Fig. 1 Structural characteristics of SiQDs. (a) TEM image; (b) HR-TEM image; (c) EDS spectrum

2.2 SiQDs 非线性特性仿真分析

体硅具有反转对称性，二阶非线性系数为零，因此无法产生 SHG。然而，Nayfeh 等[35]在含有硅纳米晶体（粒径约为 1 nm）的微晶薄膜上观察到了 SHG 信号，这种小尺寸的微型硅纳米晶体打破了晶体硅的对称性，从而提供了非零的 $\chi^{(2)}$，产生了非线性效应[36]。为了深入探究 SiQDs 具有较强 SHG 的物理机制，笔者采用 FDTD 数值模拟方法对比了同体积的单晶硅纳米颗粒（SiNP）和 SiQDs 在同种激发条件下的 SHG 信号强度，如图 2 所示。纳米颗粒的 SHG 光强[37]可以表示为

$$I_{\mathrm{SHG}} \propto f^4(\omega) f^2(2\omega) I_{\mathrm{in}}^2, \tag{1}$$

式中：I_{SHG} 和 I_{in} 分别表示 SHG 和入射光的强度；$f(\omega)$ 和 $f(2\omega)$ 分别表示基波和 SHG 频率处的场增强因

子。假设 SiQDs 的直径均为 d=2 nm，而 SiNP 的直径为 D=100 nm。本文使用的物理模型是由 108000 个直径为 2 nm 的硅纳米球组成的 SiQDs 团簇以及与 SiQDs 团簇体积相同的单个 SiNP。通过 FDTD 分别计算了 SiQDs 团簇和单个 SiNP 在基波（800 nm）和 SHG（400 nm）处的电场分布。由于入射光的波长远大于纳米粒子的直径，因此，在 800 nm 处的最大电场相当弱，进而基波的影响可以忽略不计。SiQDs 和 SiNP 的 SHG 电场分布分别如图 2（a）和图 2（b）所示，虚线表示模型结构的轮廓，入射光的偏振沿 y 方向。由图 2 可见，在 SHG（400 nm）处，SiQDs 的电场强度明显强于 SiNP。图 2（c）给出了 SiQDs 和 SiNP 的吸收谱，可见：SiQDs 和 SiNP 都在 400 nm 处有一个共振峰位，而且 SiQDs 的吸收峰值明显大于 SiNP。因此，相比于 SiNP，SiQDs 具有更强的非线性效应，即能产生更强的 SHG 信号，这使得 SiQDs 有望作为生物探针应用于生物医学成像领域。

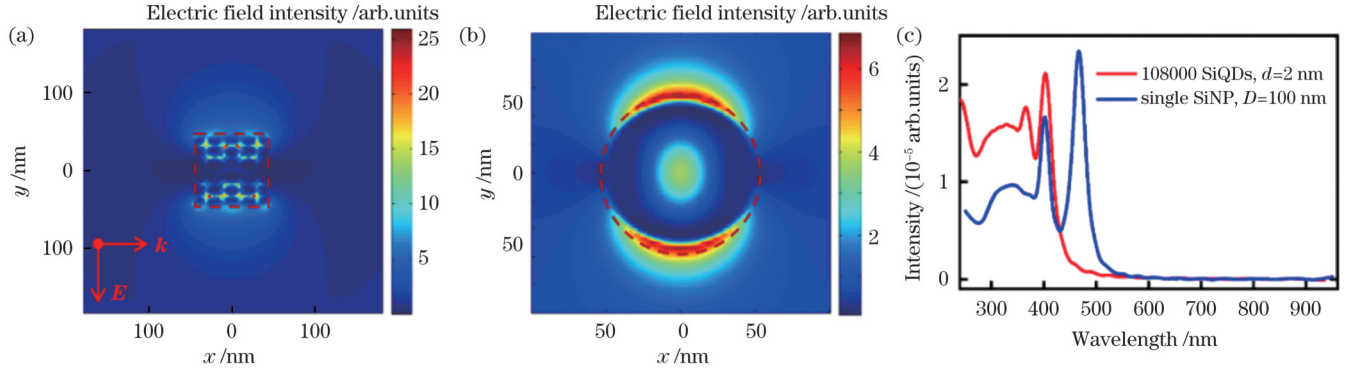

图 2　SHG 电场分布仿真结果。（a）SiQDs 的 SHG 电场分布；（b）SiNP 的 SHG 电场分布；（c）吸收谱

Fig. 2　Simulation results of SHG electric field distribution. (a) SHG electric field distribution of SiQDs; (b) SHG electric field distribution of SiNP; (c) absorption spectra

2.3　SHG 成像装置

图 3 是 SHG 成像的实验装置示意图，整个成像系统主要由光源、显微镜、探测器、计算机处理系统组成。钛宝石飞秒激光器产生波长为 800 nm、重复频率为 76 MHz、持续时间约为 120 fs 的超短脉冲光源，光源经二向色镜反射后被显微镜物镜（60×透镜，数值孔径为 0.85）聚焦在待观测样品上。样品放置在三维定位系统（P-563.3CD，Physik Instruments）上，该定位系统的各维度精度均为 1 nm。样品具有较高的二阶非线性系数，其被激发后将产生波长为 400 nm 的 SHG 信号，SHG 信号被物镜收集并透过二向色镜，然后通过分光器分别进入光电倍增管（PMT，H7244-40，Hamamatus）和光谱仪（SR500i-B1，Andor）。光电倍增管的输出信号经过锁相放大器（SR850，Standford）后被传送到数据采集系统（BNC-2120，NI）。在数据读出过程中，可使用机械快门来调整飞秒激光的曝光时间，机械快门、定位系统、数据采集系统由软件同步控制。

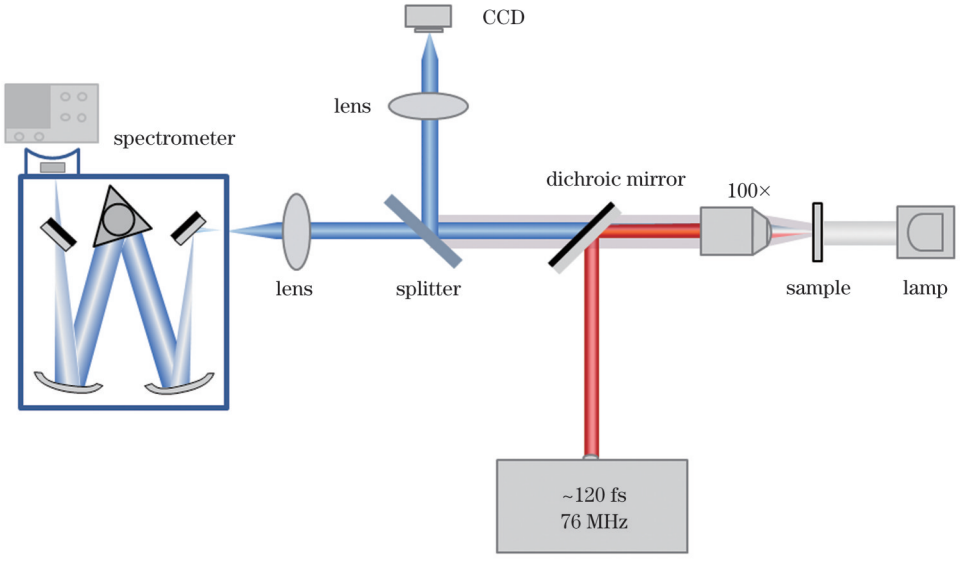

图 3　SHG 成像装置示意图

Fig. 3　Diagram of SHG imaging device

3　结果与讨论

3.1　PEG 修饰的 SiQDs 的性能测试

首先利用 SHG 成像装置研究 PEG 修饰的 SiQDs 样品的 SHG 成像特性。将 SiQDs 溶液滴在盖玻片上并使其干燥，待水蒸发后会在盖玻片上形成多个“咖啡环”，如图 4(a)所示。选取图 4(a)中的一个“咖啡环”(用虚线表示)进行 SHG 扫描成像，成像结果如图 4(b)所示，可以发现其与明场视场下的图样相同。笔者也研究了单光子激发和 SHG 激发下样品的发射光谱特性。在单光子激发条件下，当激发波长分别为 280 nm 和 322 nm 时，荧光光谱峰位分别出现在 306 nm 和 390 nm 处，如图 4(c)所示。这种受激发光对激发光波长强烈依赖的荧光特性是由不同粒径和不同表面俘获态分布导致的[38]。在波长为 800 nm 的 SHG 激发下，样品的发射光谱在 400 nm 处有一个离散的峰值，如图 4(d)所示。这表明样品具有较强的 SHG 信号，而且 SHG 信号的强度随着光源功率的增加而逐渐增强，如图 4(d)所示。为了进一步证明该信号对应二阶非线性效应，对实验数据在双自然对数坐标下进行拟合，相应的拟合结果如图 4(e)所示，拟合直线斜率约为 2.17。进一步地，

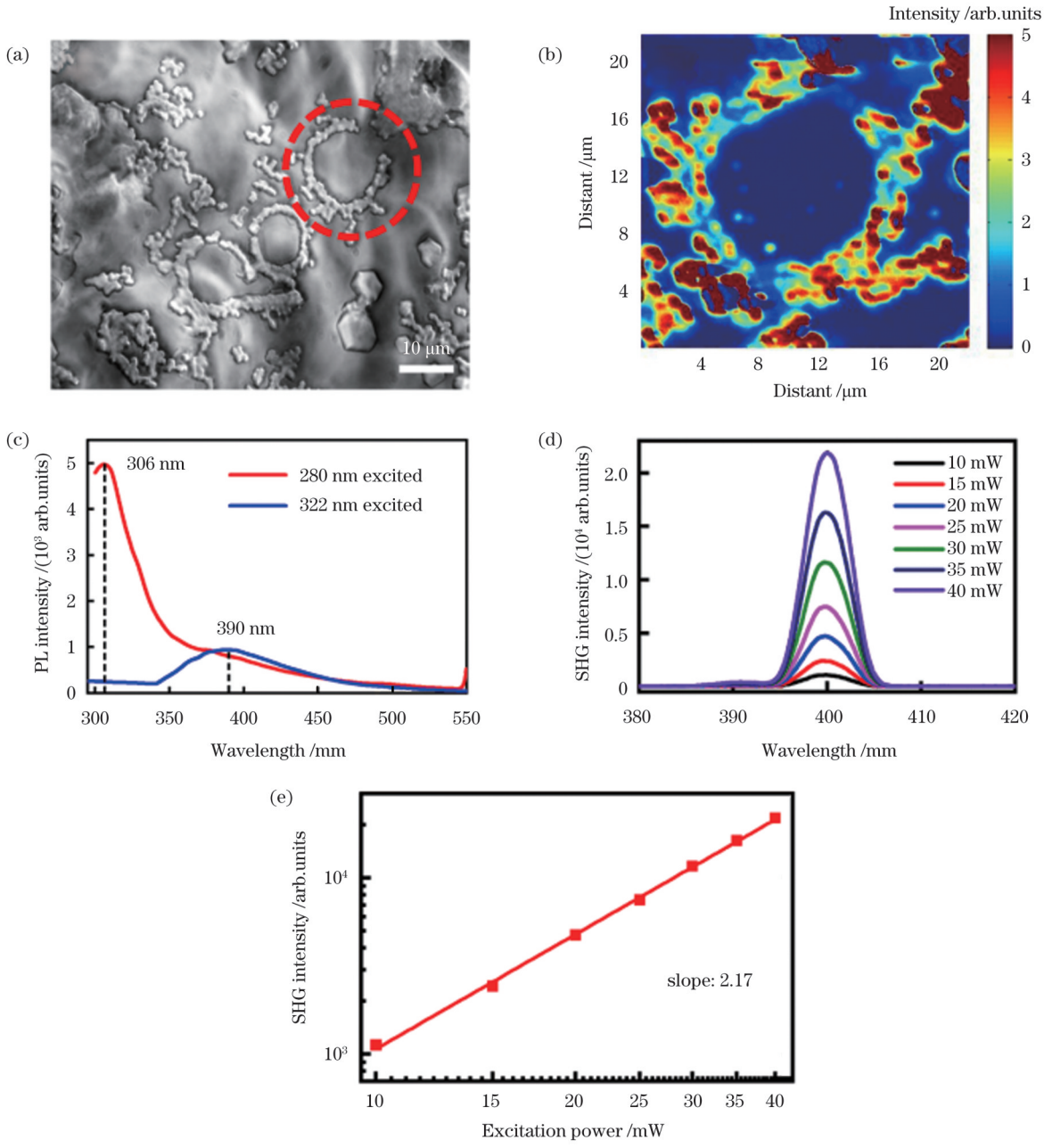

图 4　PEG 修饰的 SiQDs 的成像特性。(a)荧光成像；(b)SHG 成像；(c) 280 nm 和 322 nm 单光子激发下的荧光发射谱；(d)SHG 发射光谱图；(e)SHG 强度与激光功率的关系

Fig. 4　Imaging characteristics of PEG-coated SiQDs. (a) Fluorescence imaging; (b) SHG image; (c) fluorescence emission spectra at 280 nm and 322 nm single photon excitation; (d) SHG emission spectra; (e) relationship between SHG intensity and laser power

笔者观察到SiQDs发出的SHG信号在激光照射数小时后具有光稳定性，这是SHG成像的一个显著特点，这一特点使其在跟踪细胞谱系、监测细胞间信号传输以及研究单个细胞内分子的动态变化等方面具有重要的应用价值。

3.2 基于PEG修饰的SiQDs探针的细胞成像

为了测试使用PEG修饰的SiQDs进行细胞标记和成像的可行性，笔者开展了对HepG2细胞的SHG成像研究。将HepG2保存在含有10%胎牛血清(FBS)和0.1%二甲基亚砜(DMSO)的DMEM细胞培养基中，作为体外实验对象。在处理前一天，将细胞接种在35 mm细胞培养皿中，待细胞达到70%～80%融合度后，将其与质量浓度约为8 μg/mL的SiQDs溶液在37 ℃下孵育2 h；24 h后，用PBS缓冲液对细胞进行三次冲洗，并使用激光扫描共聚焦显微镜(蔡司LSM780 NLO)进行细胞成像。作为对照组，笔者准备了一份未与SiQDs孵育的细胞样本。实验中使用的激光发射波长为800 nm，功率密度为3 mW/μm^2，低于细胞的损伤阈值。图5(a)～(c)是经SiQDs孵育的HepG2细胞的共聚焦图像，其中图5(a)和图5(b)分别为HepG2细胞的SHG扫描图像和明场图像。在图5(a)中可以观察到大量来自样品SiQDs的SHG信号(如绿色部分所示)随机分布在HepG2细胞内部，并聚集在细胞的细胞器(如溶酶体)中。图5(c)是SHG图像[图5(a)]和明场图像[图5(b)]的叠加图。为了进行比较，对对照组的细胞进行了相同的激发操作，相应的成像结果如图5(d)～(f)所示。在图5(d)中几乎没有发现SHG信号。图5(a)～(f)所示图像都是在激光功率、增益、偏移量和扫描速度完全相同的条件下拍摄的。这些研究结果表明PEG修饰的SiQDs可以成为一个良好的SHG纳米探针，可用于生物标记与成像。

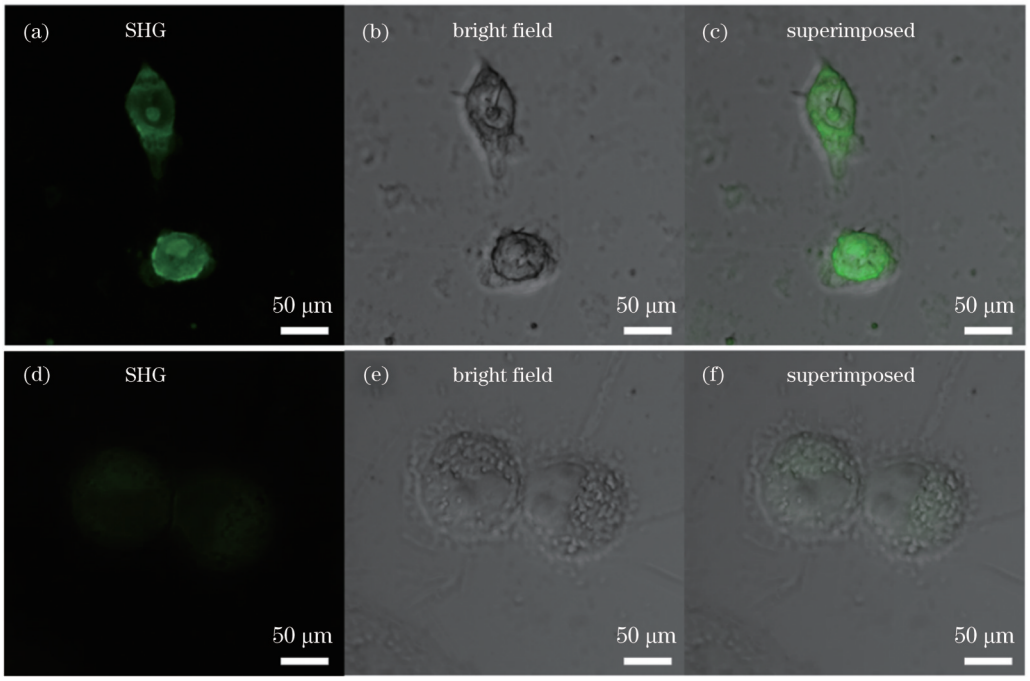

图5 HepG2细胞的共聚焦图像。(a)～(c)经过SiQDs孵育的HepG2细胞的SHG图像、明场图像和叠加图像；(d)～(f)未经过SiQDs孵育的HepG2细胞的SHG图像、明场图像、叠加图像

Fig. 5 Confocal images of HepG2 cells. (a)-(c) SHG image, bright field image and superimposed image of HepG2 cells with SiQDs incubation; (d)-(f) SHG image, bright field image and superimposed image of HepG2 cells without SiQDs incubation

接着，对经过SiQDs样品孵育的HepG2细胞进行SHG和TPL扫描成像，并对成像效果进行了比较。在800 nm波长激发下，分别在500～550 nm和395～405 nm光谱窗口范围内采集TPL信号和SHG信号。图6(a)～(c)分别显示了细胞的SHG图像以及对应的明场图像和叠加图像，图6(d)～(f)分别显示了细胞的TPL图像以及对应的明场图像和叠加图像。可以看出，SHG图像具有更高的分辨率。图6(g)～(i)和图6(j)～(l)分别显示了HepG2细胞的连续SHG和TPL时域成像效果，图像序列从左到右，时间间隔为5 s。显然，在激光的连续扫描下，TPL信号存在饱和吸收、漂白快的现象，难以实现对HepG2细胞的长时间跟踪；相比之下，SHG成像具有光稳定性，这种稳定性对于分析生物过程(如跟踪细胞谱系、监测细胞间的信号传输或单细胞内分子的动态等)至关重要。图6(m)显示样品的SHG强度约为TPL强度的100倍。本实验扫描TPL信号所需增益值是扫描SHG信号所需增益值的10倍，进一步说明了PEG修饰的SiQDs具有较强的二阶非线性效应，能够在细胞成像研究中发挥重要作用。

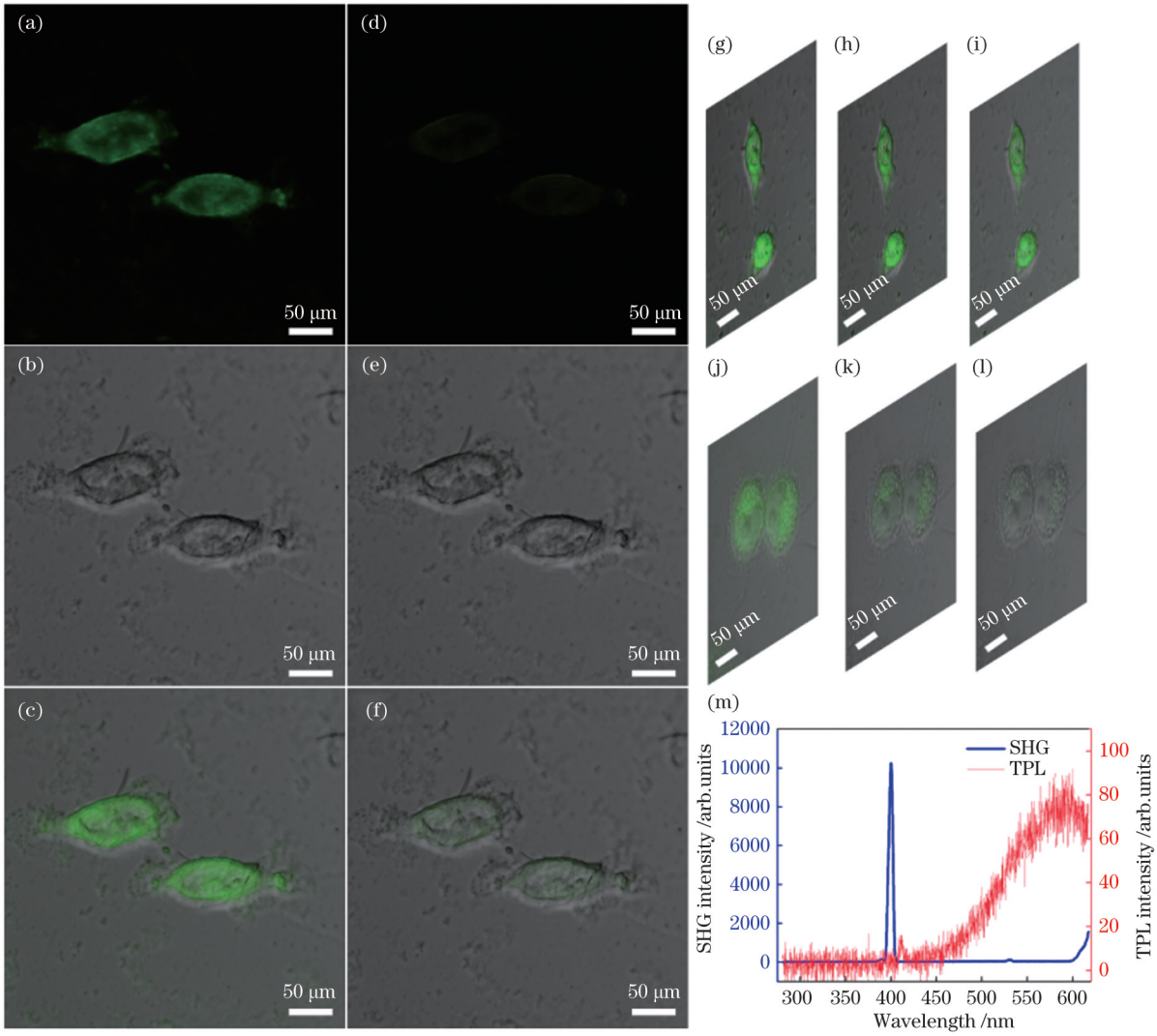

图 6 HepG2 细胞的 SHG 和 TPL 成像对比。(a)～(c)SHG 图像和对应的明场图像、叠加图像;(d)～(f)TPL 图像和对应的明场图像、叠加图像;(g)～(i)连续 SHG 成像;(j)～(l)连续 TPL 成像;(m)SHG 和 TPL 发射谱

Fig. 6 Comparison of SHG and TPL imaging in HepG2 cell. (a)–(c) SHG image and corresponding bright field image and superimposed image; (d)–(f) TPL image and corresponding bright field image and superimposed image; (g)–(i) continuous SHG imaging; (j)–(l) continuous TPL imaging; (m) SHG and TPL emission spectra

4 结 论

笔者采用还原法直接合成 PEG 修饰的 SiQDs,并从理论和实验上验证了其具有良好的二阶非线性效应,能产生较强的 SHG 信号。进一步,将其应用于人肝癌细胞(HepG2)进行非线性光学成像。成像结果表明 PEG 修饰的 SiQDs 是一种稳定可靠的生物探针,SHG 成像结果较单光子荧光成像的对比度显著提升。通过与 TPL 成像进行对比突出了 SHG 成像无漂白、无闪烁、无可饱和吸收的优点,其产生的 SHG 信号强度是 TPL 成像的 100 倍。以上结果表明基于 PEG 修饰的 SiQDs 的 SHG 成像技术在生物医学成像等领域具有广阔的应用前景。

参 考 文 献

[1] Li R, Wang X X, Zhou Y, et al. Advances in nonlinear optical microscopy for biophotonics[J]. Journal of Nanophotonics, 2018, 12(3): 033007.

[2] 张子一, 王明雪, 刘志贺, 等. 二次谐波在生物医学成像中的应用[J]. 中国激光, 2020, 47(2): 0207008.
Zhang Z Y, Wang M X, Liu Z H, et al. Application of second harmonic generation in biomedical imaging[J]. Chinese Journal of Lasers, 2020, 47(2): 0207008.

[3] Staedler D, Magouroux T, Hadji R, et al. Harmonic nanocrystals for biolabeling: a survey of optical properties and biocompatibility [J]. ACS Nano, 2012, 6(3): 2542-2549.

[4] Rice W, Kaplan D L, Georgakoudi I. Quantitative biomarkers of stem cell differentiation based on intrinsic two-photon excited fluorescence[J]. Journal of Biomedical Optics, 2007, 12(6): 060504.

[5] Duncan M D, Reintjes J, Manuccia T J. Scanning coherent anti-Stokes Raman microscope[J]. Optics Letters, 1982, 7(8): 350-352.

[6] Denk W, Strickler J H, Webb W W. Two-photon laser scanning fluorescence microscopy[J]. Science, 1990, 248(4951): 73-76.

[7] Grange R, Lanvin T, Hsieh C L, et al. Imaging with second-harmonic radiation probes in living tissue[J]. Biomedical Optics Express, 2011, 2(9): 2532-2539.

[8] Autere A, Jussila H, Dai Y Y, et al. Nonlinear optics: nonlinear optics with 2D layered materials[J]. Advanced Materials, 2018, 30 (24): 1870172.

[9] Franken P A, Hill A E, Peters C W, et al. Generation of optical harmonics[J]. Physical Review Letters, 1961, 7(4): 118-119.
[10] Dempsey W P, Fraser S E, Pantazis P. SHG nanoprobes: advancing harmonic imaging in biology[J]. BioEssays, 2012, 34(5): 351-360.
[11] Čulić -Viskota J, Dempsey W P, Fraser S E, et al. Surface functionalization of barium titanate SHG nanoprobes for *in vivo* imaging in zebrafish[J]. Nature Protocols, 2012, 7(9): 1618-1633.
[12] Fine S, Hansen W P. Optical second harmonic generation in biological systems[J]. Applied Optics, 1971, 10(10): 2350-2353.
[13] Gannaway J N, Sheppard C J R. Second-harmonic imaging in the scanning optical microscope[J]. Optical and Quantum Electronics, 1978, 10(5): 435-439.
[14] Freund I, Deutsch M, Sprecher A. Connective tissue polarity. Optical second-harmonic microscopy, crossed-beam summation, and small-angle scattering in rat-tail tendon[J]. Biophysical Journal, 1986, 50(4): 693-712.
[15] Campagnola P J, Millard A C, Terasaki M, et al. Three-dimensional high-resolution second-harmonic generation imaging of endogenous structural proteins in biological tissues[J]. Biophysical Journal, 2002, 82(1): 493-508.
[16] Nucciotti V, Stringari C, Sacconi L, et al. Probing myosin structural conformation *in vivo* by second-harmonic generation microscopy[J]. Proceedings of the National Academy of Sciences of the United States of America, 2010, 107(17): 7763-7768.
[17] Olivier N, Luengo-Oroz M A, Duloquin L, et al. Cell lineage reconstruction of early zebrafish embryos using label-free nonlinear microscopy[J]. Science, 2010, 329(5994): 967-971.
[18] Brown R M, Jr, Millard A C, Campagnola P J. Macromolecular structure of cellulose studied by second-harmonic generation imaging microscopy[J]. Optics Letters, 2003, 28(22): 2207-2209.
[19] Freund I, Deutsch M. Second-harmonic microscopy of biological tissue[J]. Optics Letters, 1986, 11(2): 94-96.
[20] 王楠楠, 高玉峰, 郑炜, 等. 基于二次谐波成像定量评估主动脉增龄性改变[J]. 中国激光, 2023, 50(15): 1507102.
Wang N N, Gao Y F, Zheng W, et al. Quantitative assessment of age-related changes in aorta based on second harmonic generation microscopy[J]. Chinese Journal of Lasers, 2023, 50(15): 1507102.
[21] Tilbury K, Campagnola P J. Applications of second-harmonic generation imaging microscopy in ovarian and breast cancer[J]. Perspectives in Medicinal Chemistry, 2015, 7: 21-32.
[22] Kim E, Steinbrück A, Buscaglia M T, et al. Second-harmonic generation of single $BaTiO_3$ nanoparticles down to 22 nm diameter [J]. ACS Nano, 2013, 7(6): 5343-5349.
[23] Bonacina L, Mugnier Y, Courvoisier F, et al. Polar $Fe(IO_3)_3$ nanocrystals as local probes for nonlinear microscopy[J]. Applied Physics B, 2007, 87(3): 399-403.
[24] Nakayama Y, Pauzauskie P J, Radenovic A, et al. Tunable nanowire nonlinear optical probe[J]. Nature, 2007, 447(7148): 1098-1101.
[25] Aufray M, Menuel S, Fort Y, et al. New synthesis of nanosized niobium oxides and lithium niobate particles and their characterization by XPS analysis[J]. Journal of Nanoscience and Nanotechnology, 2009, 9(8): 4780-4785.
[26] Johnson J C, Yan H Q, Schaller R D, et al. Near-field imaging of nonlinear optical mixing in single zinc oxide nanowires[J]. Nano Letters, 2002, 2(4): 279-283.
[27] Duan Y L, Ju C G, Yang G A, et al. Aggregation induced enhancement of linear and nonlinear optical emission from a hexaphenylene derivative[J]. Advanced Functional Materials, 2016, 26(48): 8968-8977.
[28] Chervy T, Xu J L, Duan Y L, et al. High-efficiency second-harmonic generation from hybrid light-matter states[J]. Nano Letters, 2016, 16(12): 7352-7356.
[29] Xu J L, Semin S, Niedzialek D, et al. Self-assembled organic microfibers for nonlinear optics[J]. Advanced Materials, 2013, 25 (14): 2084-2089.
[30] Pelayo García de Arquer F, Talapin D V, Klimov V I, et al. Semiconductor quantum dots: technological progress and future challenges[J]. Science, 2021, 373(6555): eaaz8541.
[31] Ghosh M, Nath S, Sen S, et al. Nonlinear optical response and characteristic Raman spectra of phagraphene quantum dots[J]. Physica Scripta, 2023, 98(4): 045109.
[32] Medintz I L, Uyeda H T, Goldman E R, et al. Quantum dot bioconjugates for imaging, labelling and sensing[J]. Nature Materials, 2005, 4(6): 435-446.
[33] Petryayeva E, Algar W R, Medintz I L. Quantum dots in bioanalysis: a review of applications across various platforms for fluorescence spectroscopy and imaging[J]. Applied Spectroscopy, 2013, 67(3): 215-252.
[34] Qi X Y, Liu H P, Guo W J, et al. New opportunities: second harmonic generation of boron-doped graphene quantum dots for stem cells imaging and ultraprecise tracking in wound healing[J]. Advanced Functional Materials, 2019, 29(37): 1902235.
[35] Nayfeh M H, Akcakir O, Belomoin G, et al. Second harmonic generation in microcrystallite films of ultrasmall Si nanoparticles[J]. Applied Physics Letters, 2000, 77(25): 4086-4088.
[36] Nayfeh M H, Rigakis N, Yamani Z. Photoexcitation of Si-Si surface states in nanocrystallites[J]. Physical Review B, 1997, 56 (4): 2079-2084.
[37] Hubert C, Billot L, Adam P M, et al. Role of surface plasmon in second harmonic generation from gold nanorods[J]. Applied Physics Letters, 2007, 90(18): 4-39.
[38] Gupta A, Swihart M T, Wiggers H. Luminescent colloidal dispersion of silicon quantum dots from microwave plasma synthesis: exploring the photoluminescence behavior across the visible spectrum[J]. Advanced Functional Materials, 2009, 19(5): 696-703.

Second Harmonic Imaging of PEG-Coated Silicon Quantum Dots in Cells

Chen Lei[1*], Xiang Jin[2], Zhao Nian[3**], Chen Tongsheng[4]

[1]*College of Physics and Optoelectronic Engineering, Foshan University, Foshan* 528000, *Guangdong, China*;
[2]*Key Laboratory of Optoelectronic Technology and Systems (Ministry of Education), College of Optoelectronic Engineering, Chongqing University, Chongqing* 400044, *China*;
[3]*College of Physics and Optoelectronics, Xiangtan University, Xiangtan* 411105, *Hunan, China*;
[4]*Guangdong Key Laboratory of Laser Life Science, College of Biophotonics, South China Normal University, Guangzhou* 510631, *Guangdong, China*

Abstract

Objective As a nonlinear optical imaging technique that offers high spatial resolution and high penetration depth, second harmonic

imaging holds great promise for clinical diagnosis and various applications in the biomedical field, because it overcomes photobleaching and saturation absorption owing to energy absorption, which are commonly encountered in fluorescence imaging. Second-harmonic generation (SHG) is a nonlinear optical process in which two identical photons interact with a nonlinear material and are effectively converted into a single photon with precisely twice the frequency of the incident beam. In biologically relevant SHG imaging, the predominant approach has traditionally relied on the use of exogenous dye markers or endogenous proteins with a relatively low SHG efficiency. In fact, numerous studies have demonstrated strong and photostable SHG signals generated by inorganic crystalline materials. However, most of these inorganic crystalline materials contain heavy metals and have relatively large sizes (~100 nm in diameter). Recently, silicon quantum dots (SiQDs) were developed and have attracted growing interest owing to their remarkable properties, such as aqueous solubility, low cytotoxicity, high quantum yield, and exceptional stability against photobleaching. However, only few studies have investigated the generation of SHG signals from SiQDs without structural reconstitution, which has great potential for advanced optical applications, particularly in the field of SHG imaging. In this study, we developed polyethylene glycol (PEG)-coated SiQDs, an asymmetric material with a high nonlinear optical effect, as second-harmonic probes. To enhance the biological affinity and reduce the surface oxidation of the SiQDs, we modified their surface with PEG and investigated the imaging effect of PEG-coated SiQDs as a biological probe for second-harmonic wave imaging in HepG2 cells. Compared to two-photon fluorescence imaging, the second-harmonic imaging technique based on PEG-coated SiQDs provides more reliable and stable results. This finding can promote the future applications of SiQDs in molecular imaging, drug delivery, and stem cell therapy. By combining the advantages of the SHG dye, which has good biocompatibility and extremely low cytotoxicity, and the SHG inorganic crystalline materials with the photostability of the crystal structure, our SiQDs are expected to become the primary choice among many probes. We labeled hepatocellular carcinoma (HepG2) cells with non-functionalized SiQDs for cell imaging using SHG.

Methods First, the nonlinear material used in this study, PEG-coated SiQDs, was synthesized by directly reducing the precursor with silicon-oxygen bonds and then modifying with organic ligands. The morphology and chemical composition of the SiQDs were characterized through transmission electron microscopy (TEM) and energy-dispersive X-ray spectroscopy (EDS). Furthermore, the physical mechanism behind the strong SHG of SiQDs was examined using finite-difference time-domain (FDTD) numerical simulations. The second harmonic characteristics of the SiQDs were then evaluated experimentally using a custom-built setup. Finally, to verify the feasibility of using the PEG-coated SiQDs in cell labeling and imaging, SHG imaging studies on HepG2 cells were conducted using confocal microscopy.

Results and Discussions The TEM image of the PEG-coated SiQDs [Fig. 1(a)] reveals that they are approximately spherical and have an average diameter of (2±0.5) nm. The excellent second-order nonlinear effects of these SiQDs were verified both theoretically and experimentally. By scanning the SHG signals of the SiQDs [see Fig. 4(b)], we confirmed that they exhibit strong and stable SHG signals. Furthermore, we used these SiQDs to perform nonlinear optical imaging of HepG2 cells. Confocal microscopic visualization of the HepG2 cells treated with PEG-coated SiQDs confirmed the excellent tracking and imaging ability of the SiQDs (Fig. 5). Furthermore, a TPL scan of the cells incubated with SiQDs demonstrated the advantages of SHG imaging over TPL imaging (Fig. 6). Overall, the PEG-coated SiQDs serve as stable and reliable biological probes, significantly improving the image contrast compared with that of two-photon fluorescence imaging. The advantages of SHG imaging, including the absence of photobleaching, blinking, and saturation absorption, are highlighted. In addition, the intensity of the SHG signal produced by the PEG-coated SiQDs is 100 times higher than that obtained in two-photon fluorescence imaging [Fig. 6(m)]. These results indicate that SHG imaging based on PEG-coated SiQDs has great potential for a wide range of applications in biomedical imaging and other related fields.

Conclusions This paper presents a method for preparing PEG-coated SiQDs and their application in cell imaging. The PEG-coated SiQDs have a dynamic fluid diameter of only (2±0.5) nm, and the PEG molecules on their surface enhance their biocompatibility and show no apparent toxicity. The main innovation lies in the exceptionally strong and stable SHG signals exhibited by SiQDs. The SiQDs were employed as biological probes for SHG imaging of human liver cancer cells (HepG2). The advantages of SHG imaging, including the absence of photobleaching, blinking, and saturation absorption, were highlighted by comparing the results with those of two-photon fluorescence imaging. Thus, SiQDs can serve as highly biocompatible photosensitizers without causing toxic side effects and thus have promising prospects in biomedical applications.

Key words nonlinear optics; second harmonic imaging; silicon quantum dots; human liver cancer cells; biological probe